Materials Research Proceedings 28 (2023) 737-746 https://doi.org/10.21741/9781644902479-80

Improved failure characterisation of high-strength steel using a butterfly test rig with rotation control

STOCKBURGER Eugen[1,a,*], WESTER Hendrik[1,b], JEGATHEESWARAN Vithusaan[1,c], DYKIERT Matthäus[1,d] and BEHRENS Bernd-Arno[1,e]

[1]Institute of Forming Technology and Machines (IFUM), Leibniz Universität Hannover, An der Universität 2, 30823 Garbsen, Germany

[a]stockburger@ifum.uni-hannover.de, [b]wester@ifum.uni-hannover.de, [c]jegatheeswaran@ifum.uni-hannover.de, [d]dykiert@ifum.uni-hannover.de, [e]behrens@ifum.uni-hannover.de

Keywords: CP800, Butterfly Specimen, Experimental-Numerical Procedure

Abstract. A forming limit diagram is the standard method to describe the forming capacity of sheet materials. It predicts failure due to necking by limiting major and minor strains. For failure due to fracture, the fracture forming limit diagram is used, but fracture caused by plastic deformation at a shear-dominated stress state cannot be predicted with a conventional fracture forming limit diagram. Therefore, stress-based failure models are used as an alternative. These models are describing the fracture of sheet materials based on the failure strain and the stress state. Material-specific parameters must be determined, but a standardised procedure for the calibration of stress-based failure models is currently not established. Most test procedures show non-constant stress paths and varying stress states in the crack initiation area, which leads to uncertainties and inaccuracies for modelling. Therefore, a new test methodology was invented at the IFUM: a prior presented butterfly test rig was extended to enable an online rotation to adapt the loading angle while testing. First, butterfly tests with CP800 were performed for three fixed loading conditions. The tests were modelled numerically with boundary conditions corresponding to the tests. Based on the numerical results, the stress state as well as failure strain were identified and the stress state deviations were calculated. Afterwards, the necessary angular displacements to compensate the stress state deviations for the adaptive test rig were iteratively determined with numerical simulations using an automatised Python script. Finally, the butterfly tests were performed experimentally with the determined adaptive loading angles to identify the specimen failure and compared to the simulations for validation.

Introduction

The forming limit diagram (FLD) defines the critical major and minor strains of a sheet metal, which lead to material failure if exceeded. The FLD is conventionally used to describe forming limits due to necking. Failure due to fracture can be described with the fracture forming limit diagram (FFLD). However, the FLD and the FFLD give an inadequate prediction of the failure for high-strength steel (HSS) sheets, since it is valid for linear strain paths and for the strain states between uniaxial tension and biaxial tension [1]. Modern forming processes and HSS sheets often show non-linear strain paths. Furthermore, failure due to fracture initiation caused by plastic deformation at a shear-dominated stress state cannot be predicted by the FLD or the FFLD [2]. As an alternative to the FFLD, failure models based on the stress state are used. Those failure models describe the failure of the sheet metal under consideration of the stress state by means of the stress-state-dependent equivalent plastic strain at failure ε_f, which allows statements in the case of non-linear strain paths and shear-dominated stress states. To describe the three-dimensional stress state,

Materials Research Proceedings 28 (2023) 737-746 https://doi.org/10.21741/9781644902479-80

the stress triaxiality η and the normalised Lode angle θ are used. A common stress-based model is the Modified Mohr-Coulomb (MMC) failure model [3], which can be written as

$$\varepsilon_{f,MMC} = \left[c_1 \cdot \left(\eta + \frac{1}{3} \cdot sin\left(\frac{\theta\pi}{6}\right) \right) + c_2 \cdot \left(\sqrt{\frac{1+c_1^2}{3}} \cdot cos\left(\frac{\theta\pi}{6}\right) \right) \right]^{-\frac{1}{n}} \quad (1)$$

whereby c_1, c_2 and n are material-specific parameters. For the calibration of the failure models, failure characterisation experiments are performed, but a standardised procedure for testing and calibrating is currently not available. Used failure characterisation experiments mostly result in non-constant stress paths in the area of the specimen failure [4]. In Fig. 1 (A) common failure characterisation specimen such as the Miyauchi, holed tensile as well as waisted tensile specimen are shown and in Fig. 1 (B) the corresponding non-constant stress paths are visible from those specimens. Only the hydraulic bulge test leads to a constant stress path. In order to minimise the resulting uncertainties and inaccuracies of the failure characterisation for stress-based failure models, a new experimental-numerical testing methodology for an improved failure characterisation with constant stress paths is engineered and presented within the scope of this work.

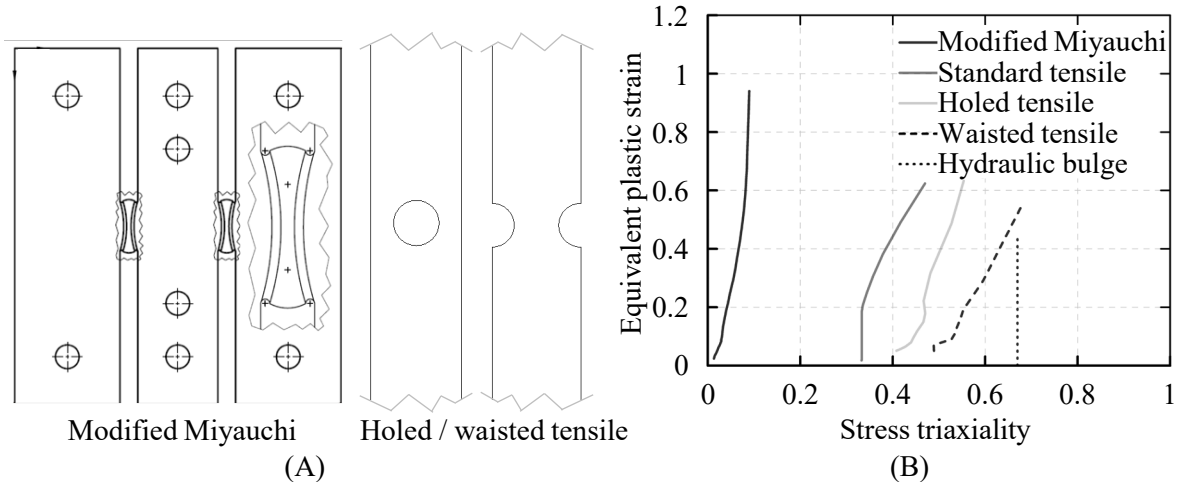

Fig. 1. Failure characterisation specimen and resulting non-constant stress paths based on the work from Behrens et al. [4].

New Experimental-Numerical Failure Characterisation Methodology

The module for the new adaptive test methodology is based on a prior developed test module shown by Stockburger et al. in [5]. In this test module, according to the test principle of Arcan et al. [6], a butterfly specimen can be tested under different orientations or loading angles α to the normal loading direction of the tensile testing machine, whereby different stress states can be achieved in the test area of the specimen. Using the butterfly specimen has the advantage compared to conventional failure characterisation specimen that the specimen failure is not initialised at the specimen edge, but in the centre of the specimen. Nevertheless, as for other specimen the stress paths of the butterfly specimens are not entirely constant. To estimate the characteristic stress state and the equivalent plastic strain at failure which is needed to calibrate models like the MMC failure model, the butterfly specimen must be numerically modelled considering boundary conditions from the experiments.

Materials Research Proceedings 28 (2023) 737-746 https://doi.org/10.21741/9781644902479-80

In order to solve the problem of non-constant stress paths in the experiment, a new adaptive test module was developed. Fig. 2 shows an illustration of the module for the new adaptive test methodology. The new test module consists of two separate specimen holders, which each have an outer ring gear and a recess for the butterfly specimen. Two mounting plates are used to attach the butterfly specimen to the specimen holder. The outer ring gears from the upper and lower specimen holders are each in contact with a worm shaft, while the upper and lower worm shafts are connected to two electric motors by two bevel gears. A rotational movement of the specimen holders is generated when the electric motors are activated and thus the current loading angle α can be changed by an adaptive loading angle α_{adap}. The rotation is regulated by a control device with a sensor, that determines the angular position. The entire test module is attached to a tensile testing machine by means of two connecting plates. Overall, the tensile testing machine is applying the load, which is transferred from the two separate specimen holders to the butterfly specimen. With the presented testing module, loading angles α are continuously adjustable during testing in order to obtain constant stress states.

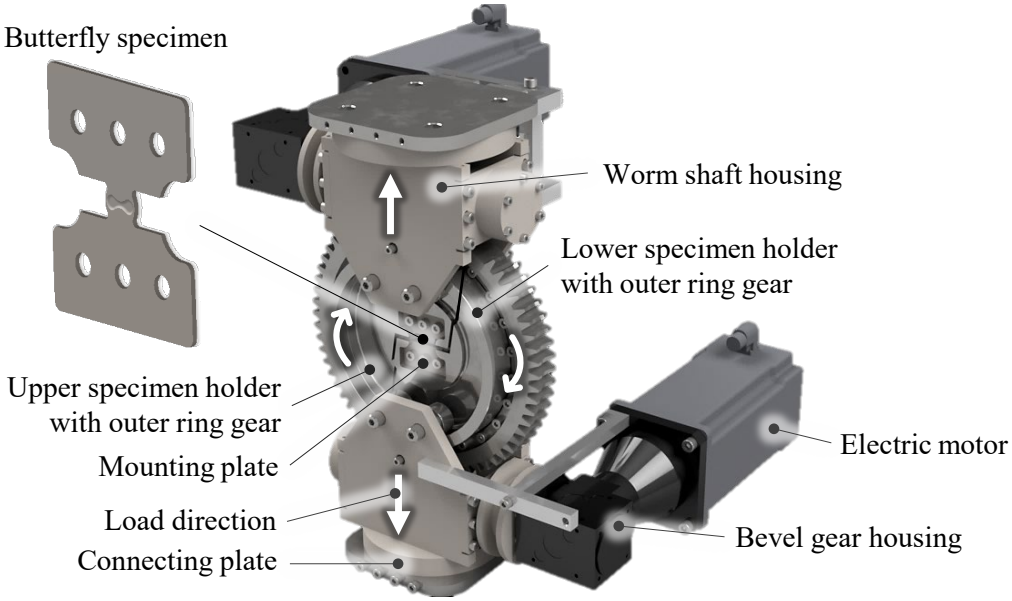

Fig. 2. Module for the new adaptive test method with butterfly specimen.

The design of the adaption loading angle α_{adap} is carried out iteratively with the aid of a numerical model of the test module. For this purpose, tests with a fixed loading condition α are first carried out experimentally and then mapped numerically. The experimental displacements up to specimen failure serve as boundary conditions for the simulation model, which is shown in Fig. 3 (A). Based on the results, the required adaption loading angle α_{adap} is now calculated numerically. For this purpose, the adaption loading angle α_{adap} is varied automatically within a sensitivity study using a Python script as shown in Fig 3 (B). First, a variation range of the adaption loading angle α_{adap} and the step size of it is specified. Consequently, a simulation is carried out iteratively for each adaption loading angle α_{adap} in the variation range. In order to determine the time of the angle adaption at which the simulations start, the stress triaxiality is taken as an indicator. The maximal deviation of the stress triaxiality was subjectively defined as 0.03. As soon as the equivalent plastic strain-stress triaxiality path showed a change higher than the maximal deviation, the iterative simulations for the adaption loading angle α_{adap} begin. Depending on the outcome, the procedure is repeated for further adaption. After the numerical design, experimental tests are performed using the numerically-iterative determined angle adaption. Those results are

used to identify the material failure under constant stress states and to verify the numerical procedure. Finally, the MMC failure model can be calibrated as well as compared for the fixed and the new adaptive test methodology.

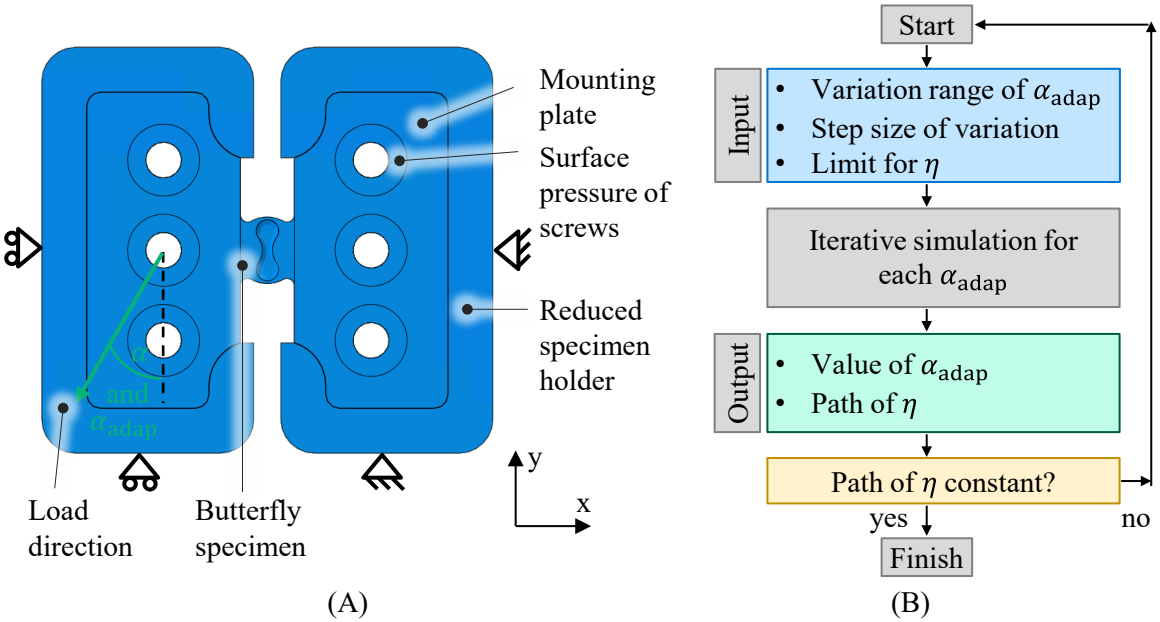

Fig. 3. Simulation model of the butterfly tests (A) and sequence plan of the Python script (B).

Application of the New Failure Characterisation Methodology

The new failure characterisation methodology was applied to the complex-phase HSS CR570Y780T-CP (CP800) from voestalpine Stahl GmbH. The outer contour of the specimen was cut by waterjet and the thickness reduction in the examination area of the specimen was carried out by milling. The new butterfly test module was installed in the tensile testing machine S100/ZD from DYNA-MESS Prüfsysteme GmbH. First, butterfly tests for the fixed configuration of the loading angles -3°, 28° and 74.5° were performed. For measuring the specimen displacement and estimation of fracture occurrence in the examination area, the optical measurement system Aramis from Carl Zeiss GOM Metrology GmbH was used. For each loading angle the tests were repeated three times. The testing temperature corresponded to room temperature and the testing speed was set to 0.05 mm/s.

Afterwards, the experiments with fixed loading conditions were numerically modelled to estimate the equivalent plastic strain at failure and the stress triaxiality as well as the normalised Lode angle paths. The FE models were generated in Abaqus/Standard for each loading angle with the corresponding displacements until failure in x- and y-direction from the experiments. The boundary conditions were extracted from the optical measurements using digital image correlation and directly applied to the specimen holder. The elastic behaviour of the material was described with a modulus of elasticity of 210 GPa and a Poisson's ratio of 0.3. The data required for modelling the plastic flow behaviour, such as flow curve and anisotropy parameters, are summarised in Table 1 and were previously published by Behrens et al. in [7]. The hardening behaviour was modelled by the Hockett-Sherby approach [8] and the anisotropy by the Hill48 yield function [9]. The Hockett-Sherby approach describes the flow stress k_f of the material as a function of the equivalent plastic strain ε and the four material parameters a, b, c as well as d. The specimen holder was geometrically reduced and modelled as rigid body with 210 GPa as elastic modulus and 0.3 as Poisson's ratio. A discretisation of the specimen was done with linear reduced-integrated hexahedral elements with hourglass control, referred to as C3D8R in Abaqus. The examination area of the specimens was meshed with an element edge length of 0.1 mm and the

thickness of the specimens by five elements. The surface pressures of the screws acting on the mounting plates were modelled with a surface pressure of 204 MPa, which results from the tightening torque of the screws.

Table 1. Parameters for the extrapolation approach and anisotropy function from [7].

	Equation		***a* in MPa**	***b* in MPa**	***c***	***d***
Hockett-Sherby	$k_f = a - (a - b) \cdot e^{c \cdot \varepsilon^d}$ (2)		4.96 E-05	502.5	0.823	0.170
	F	***G***	***H***	***L***	***M***	***N***
Hill'48	0.495	0.531	0.469	1.5	1.5	1.634

Further, the numerical models were evaluated with regard to the equivalent plastic strain, the stress triaxiality path and the normalised Lode angle path. The models were analysed on the surface of the investigation area. The equivalent plastic strain was plotted as a function of the triaxiality and of the normalised Lode angle. Based on these curves, the characteristic stress state was calculated by the area-weighted centroid. The equivalent plastic strain at failure and the characteristic stress state from the fixed configuration are later compared to the values of the adaptive tests.

Next, the design of the adaption loading angle α_{adap} was carried out. The procedure is shown in Fig. 4 exemplarily for the adaptions of the loading angle 28°. First, the course of the equivalent plastic strain-stress triaxiality curve for the fixed loading condition α was considered. Based on the illustrated curve, a value for the stress triaxiality was manually selected, at which the angular adaption begins. When selecting the limit value, care was taken to intervene early enough to correct the curve with regard to a more constant path. In Fig. 4 (A), the limit value is marked orange at a stress triaxiality of 0.135. Now the Python script was used to design the angle adaption. During pre-processing, only the displacement boundary conditions were automatised redefined by a subroutine to change the loading. With the changed input variables, the simulation was proceeded. In the example given, the adaption loading angle α_{adap} was varied between 5° and 6°. The corresponding influence of the angle adaption on the stress state is displayed in Fig. 4 (B). 6° was selected as the adaption loading angle α_{adap} and the limit for the stress triaxiality was set to 0.139. When choosing the values, care was taken again to ensure that the path remains as constant as possible.

Materials Research Proceedings 28 (2023) 737-746 https://doi.org/10.21741/9781644902479-80

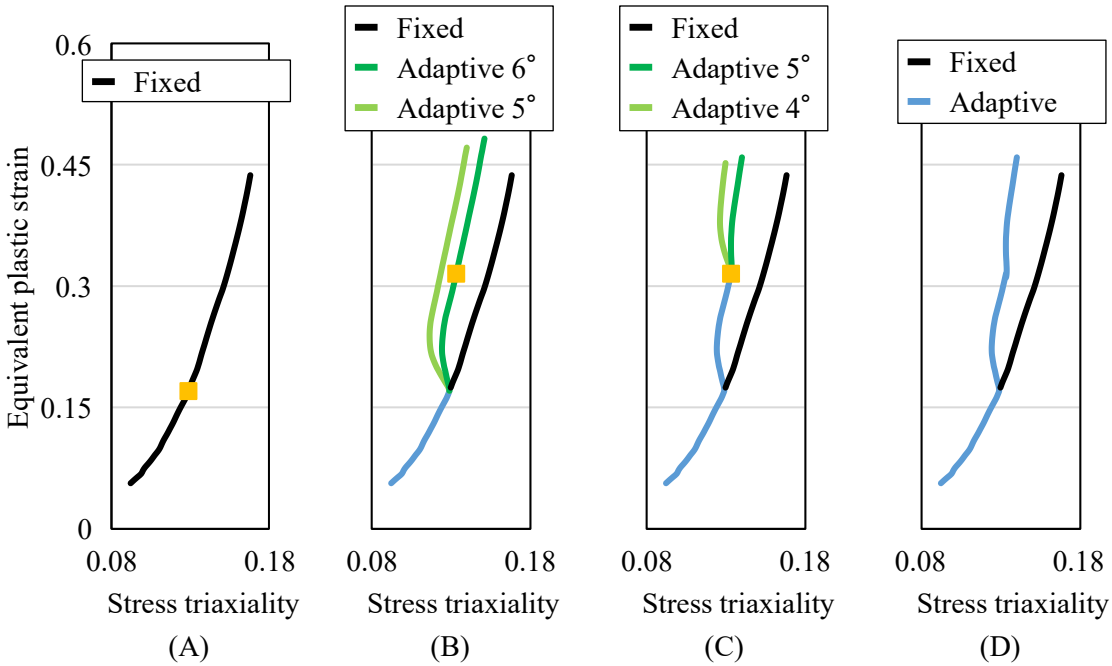

Fig. 4. Iterative design of the angular adaptions for the loading angle 28°.

In order to design the second angle adaption, a next adaption loading angle α_{adap} were chosen manually. Now the subroutine proceeded further in the same way as for the first angle adaption. Next, the adaption loading angle α_{adap} 4° and 5° were compared. The equivalent plastic strain-stress triaxiality paths after the second angle adaption are illustrated in Fig. 4 (C). With regard to a constant curve, the adaption loading angle α_{adap} of 5° was selected. Fig. 4 (D) compares the final equivalent plastic strain-stress triaxiality path of the designed adaptive test for a loading angle α of 28° with the path for a fixed loading condition α.

Additionally, butterfly experiments with the designed angular adaptions were carried out with the new butterfly test module for the three loading angles α -3°, 28° and 74.5°. Here, the limit values for the stress triaxialities served as boundary conditions with displacements in x- and y-direction. A comparison of the experimental and numerical force-displacement curves for the adaptive test methodology is shown in Fig. 5 (A). The comparison shows that the properties as well as boundary conditions used to describe the flow behaviour and the structure of the FE model represented the experimental tests sufficiently accurate and were therefore considered validated in this range. Based on the comparison, the models were considered suitable for the evaluation of the stress state. For increasing the loading angle, the force rises and the displacement until failure reduces.

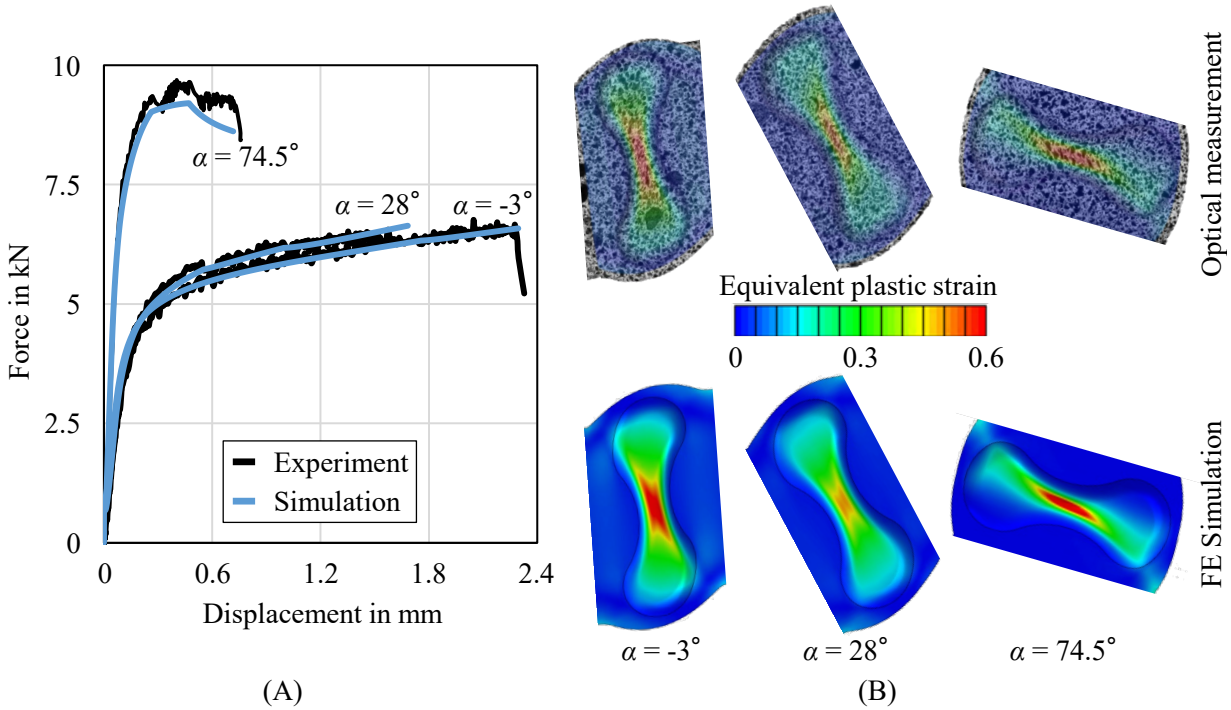

Fig. 5. Comparison of the experimental as well as numerical force-displacement curves (A) and equivalent plastic strain distribution of the butterfly specimen (B) for the adaptive test methodology.

Fig. 5 (B) illustrates the equivalent plastic strain distribution directly before failure of the butterfly tests with the adaptive test methodology. The deformation is accumulated in the centre of all three specimen for both, the experiments and the simulations. Comparing the optical measurement from the experiments and simulation results, the equivalent plastic strain distribution is very similar. In general, the equivalent plastic strain reduces from a loading angle of -3° to 28° and rises again for 74.5°. In the centre of the specimen, the equivalent plastic strain and the stress state were further evaluated.

Fig. 6 (A) illustrates the comparison of the numerically determined equivalent plastic strain-stress triaxiality paths at the location of fracture initiation. It shows that the angular adaptions in the adaptive tests compared to the tests with fixed loading condition α result in significantly more constant paths with regard to the equivalent plastic strain-stress triaxiality path. Further, it is evident in Fig. 6 (A) that higher equivalent plastic strains are achieved in the adaptive tests compared to the fixed tests. This is due to higher displacements until failure for the adaptive tests. This is also shown in the comparison of the characteristic stress states in Fig. 6 (B). Due to the more constant equivalent plastic strain-stress triaxiality path in the adaptive tests, smaller characteristic values are achieved than in the fixed tests. This is due to the fact that the area under the curves decreases because of the more constant stress path. As a result, the centre of gravity of the area shifts to smaller values and the characteristic values decrease. In the tests with a fixed loading condition α, the stress state change during the tests is large and non-constant stress paths are present.

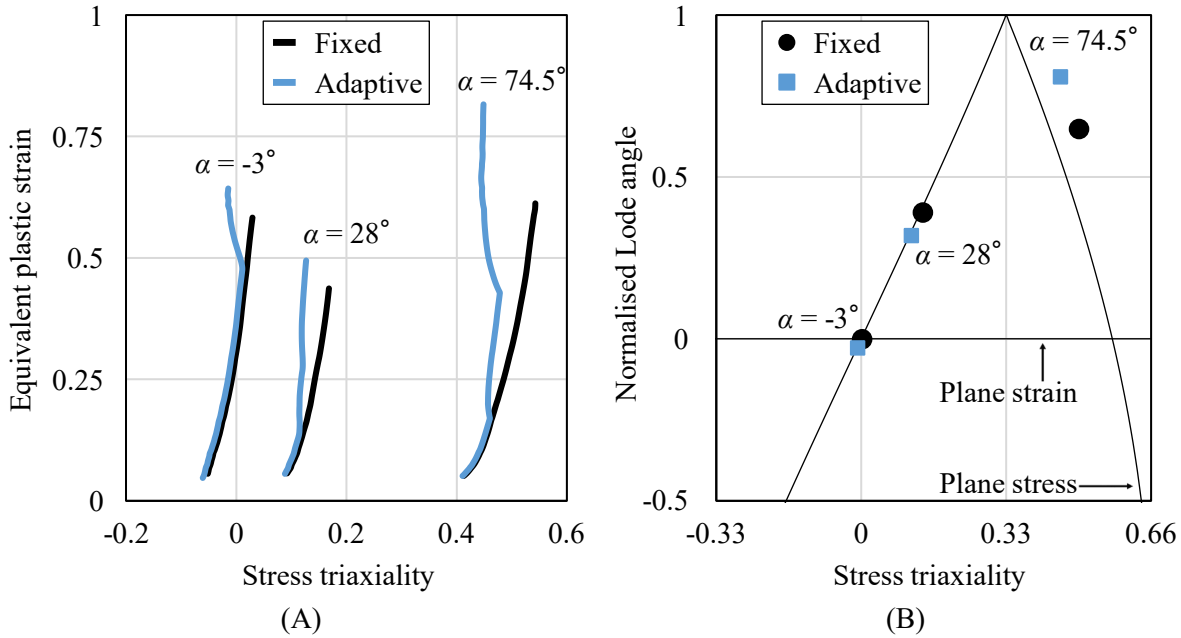

Fig. 6. Equivalent plastic strain-stress triaxiality paths (A) and characteristic stress states (B) for the fixed and adaptive test methodology.

A comparison of the calibrated MMC failure models for the test methodology with fixed loading condition α and for the new adaptive test methodology is presented in Fig. 7. The failure models are shown for plane stress in Fig. 7 (A) and plane strain state in Fig. 7 (B). The failure curves in the plane stress and plane strain state are of similar course for both methods. The major difference is the higher level of the failure curve achieved with the adaptive test methodology due to higher equivalent plastic strains of each test. A minor difference is that the failure curve from the fixed test methodology has a lower slope than the failure curve of the adaptive test methodology. Anyway, the higher accuracy of the failure model for the adaptive test methodology compared to the fixed test methodology needs to be proven by the simulation of forming processes, which is planned for future investigations.

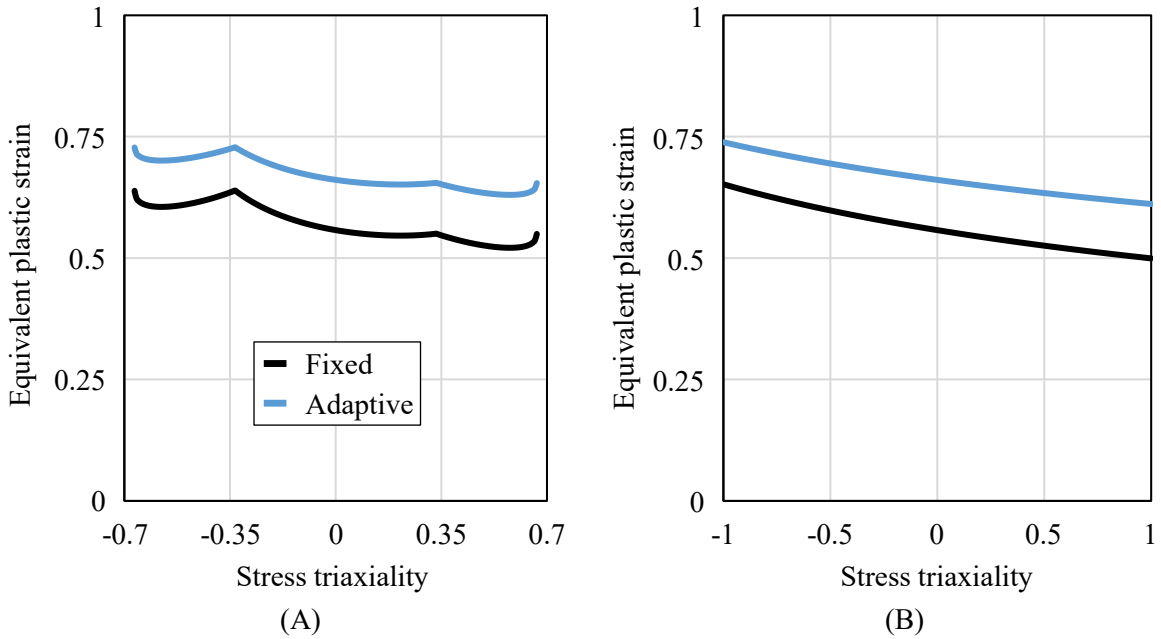

Fig. 7. Plane stress (A) and plane strain state (B) of the fitted MMC-model for the fixed and adaptive test methodology.

Summary

In this work a new experimental-numerical failure characterisation methodology is presented. Conventional failure characterisation tests show a non-constant stress path and therefore inaccuracies for modelling. Butterfly tests for the fixed loading conditions -3°, 28° and 74.5° were performed and numerically modelled. Based on the results for the stress path of the simulations, angle adaptions while testing were iteratively-numerical determined to correct the stress path into a constant path. Afterwards, butterfly experiments were performed using the estimated adaptive angles and compared to the simulations. Therefore, it was possible to achieve a more constant stress path and to minimise the change in the stress state at the location of fracture. Finally, MMC failure model were calibrated for both methodologies and compared to each other, which showed the influence of the new failure characterisation methodology.

In future investigations, more loading angles for the butterfly tests will be experimentally performed and numerically modelled to enhance the data for the failure model parametrisations. Further, it is planned to optimise the Python script to estimate the angle adaptions not subjectively anymore but automatically based on general criteria. Then, demonstrators in the style of a B-pillar as shown in [10] will be experimentally produced and the tests will be reproduced numerically using the MMC failure models from the fixed as well as adaptive test methodology. Based on the results, the failure prediction of the new adaptive test methodology will be evaluated regarding its potential for a higher accurate failure modelling.

Acknowledgements

The authors would like to thank the German Research Foundation (Deutsche Forschungsgemeinschaft, DFG) for the financial and organisational support of this project with the number 405334714. Furthermore, the authors would like to thank voestalpine Stahl GmbH for providing the material under investigation.

References

[1] Standard ISO 6892-1:2020-06, Metallic materials - Tensile testing – Part 1: Method of test at room temperature, Beuth Verlag GmbH, Berlin, Germany, 2020.

[2] Y. Li, M. Luo, J. Gerlach, T. Wierzbicki, Prediction of shear-induced fracture in sheet metal forming, J. Mat. Proc. Tech. 210 (2010) 1858-1869. https://doi.org/10.1016/j.jmatprotec.2010.06.021
[3] Y. Bai, T. Wierzbicki, A new model of metal plasticity and fracture with pressure and Lode dependence, Int. J. Plast. 24-6 (2008) 1071-1096. https://doi.org/10.1016/j.ijplas.2007.09.004
[4] B.-A. Behrens, A. Bouguecha, M. Vucetic, I. Peshekhodov, Characterisation of the quasi-static flow and fracture behaviour of dual-phase steel sheets in a wide range of plane stress states, Arch. Civil Mech. Eng. 12 (2012) 397-406. https://doi.org/10.1016/j.acme.2012.06.017
[5] E. Stockburger, H. Vogt, H. Wester, S. Hübner, B.-A. Behrens, Evaluating Material Failure of AHSS Using Acoustic Emission Analysis, Mat. Res. Proc. 25 (2023) 379-386. https://doi.org/10.21741/9781644902417-47
[6] M. Arcan, Z. Hashin, A. Voloshin, A method to produce uniform plane-stress states with applications to fiber-reinforced materials, Exp. Mech. 18 (1978) 141-146. https://doi.org/10.1007/BF02324146
[7] B.-A. Behrens, K. Brunotte, H. Wester, M. Dykiert, Fracture Characterisation by Butterfly-Tests and Damage Modelling of Advanced High Strength Steels, Key Eng. Mat. 883 (2021) 294-302. https://doi.org/10.4028/www.scientific.net/kem.883.294
[8] J.E. Hockett, O.D. Sherby, Large strain deformation of polycrystalline metals at low homologous temperatures, J. Mech. Phys. Solid. 23 (1975) 87-98. https://doi.org/10.1016/0022-5096(75)90018-6
[9] R.A Hill, Theory of the yielding and plastic flow of anisotropic metals, Proc. R. Soc. A 193 (1948) 281-297. https://doi.org/10.1098/rspa.1948.0045
[10] B.-A. Behrens, S. Jüttner, K. Brunotte, F. Özkaya, M. Wohner, E. Stockburger, Extension of the Conventional Press Hardening Process by Local Material Influence to Improve Joining Ability, Proc. Manuf. 47 (2020) 1345-1352. https://doi.org/10.1016/j.promfg.2020.04.258